JOURNAL OF MATERIALS SCIENCE 32 (1997) 2255–2261

Synthesis of α''-$Fe_{16}N_2$ iron nitride by means of nitrogen-ion implantation into iron thin films

H. SHINNO, M. UEHARA, K. SAITO
National Research Institute for Metals 1-2-1, Sengen, Tsukuba-shi, Ibaraki 305, Japan

Nitrogen ions were implanted into [1 0 0] oriented α-Fe thin films on MgO (1 0 0) substrates at room temperature. The films were annealed at a low temperature of 473 K. α''-$Fe_{16}N_2$ and α'-martensite phases were formed and the volume fractions of these nitride phases were estimated from the X-ray diffraction patterns. When the film thickness was 250 nm, α''-$Fe_{16}N_2$ was formed directly by ion implantation and the maximum volume fraction was about 12%. For the case of 50 nm thick films, no α''-$Fe_{16}N_2$ but α'-martensite was formed after nitrogen-ion implantation, and the volume fraction of the martensite exceeded 90%. By post annealing at 473 K, α''-$Fe_{16}N_2$ was formed, when the implanted specimens were coated with gold or copper films. The volume fraction of α''-$Fe_{16}N_2$ reached about 36%. A SQUID magnetic measurement showed that the saturation magnetization of the nitrogen-implanted 250 nm thick iron films was a few per cent larger than that of unimplanted iron films.

1. Introduction

Kim and Takahashi [1] have reported that iron nitride films prepared by reactive-vapour deposition contained α''-$Fe_{16}N_2$, exhibiting large saturation magnetization as large as 2.8 μ_B per iron atom. Since then, α''-$Fe_{16}N_2$ nitride has become known as one of the most interesting magnetic materials and many researchers have tried to synthesize it by vapour deposition, sputtering, and ion implantation, but failed in obtaining such a giant magnetization of the nitride [2, 3]. Thereafter, in 1991, Komuro *et al.* [4, 5] succeeded in preparing a single crystal of α''-$Fe_{16}N_2$ by MBE and have shown the saturated magnetization of 3 μ_B per iron atom. Similar, but somewhat smaller, saturation magnetizations have also been observed in specimens prepared by gas nitrification [6], reactive sputtering [7, 8] and ion implantation [9–13].

On the other hand, it has been shown that electron band theory cannot explain a giant magnetization, but only predicts 2.4 μ_B per iron atom for the saturation magnetization of α''-$Fe_{16}N_2$ [14, 15].

The present study aimed to elucidate optimum conditions for synthesizing the metastable α''-$Fe_{16}N_2$ phase by nitrogen-ion implantation into iron films. Ion implantation is a unique method for implanting atoms and creating metastable phases without any thermodynamical restrictions. In particular, we can control the depth profile of the nitrogen concentration in thin films by multiple implantation, i.e. by changing ion energies and ion doses.

2. Experimental procedure

α-Fe thin films of 250 and 50 nm thicknesses were deposited by r.f. sputtering on an MgO(1 0 0) surface at a substrate temperature of 723 K. The target material used was 99.99% pure iron. The argon pressure was between 1.3 and 4 Pa and r.f. power was 700 W. The deposited films exhibited strong [1 0 0] preferred orientation perpendicular to the film surface. The film thickness was measured by using a mechanical stylus.

Nitrogen ions were implanted into the iron films at room temperature. Multi-step ion implantation was performed using N^+ and N_2^+ ions with various energies, to obtain the desired depth distribution of nitrogen concentration in the iron films. Because the iron films were highly oriented, ion beams were irradiated at an angle of 6° inclined to the normal of the film surface to avoid channelling effects. The nitrogen-implanted specimens were annealed in vacuum in order to transform α'-martensite to α''-$Fe_{16}N_2$. Samples 50 nm thick were coated with gold- or copper-deposited films before annealing to confine nitrogen to the films during annealing. The thickness of the coating films was about 50 nm.

The specimens were characterized by X-ray diffraction (XRD) using CuK_α. The volume fractions of α''-$Fe_{16}N_2$, α'-martensite and α-Fe were estimated from the relative integrated intensities of each diffraction peak. In the case of the gold-coated specimen, the volume fractions were not evaluated, because the XRD peak of Au(2 2 0) overlapped that of α-Fe(2 0 0). Magnetic hysteresis curves were measured for nitrogen-implanted and unimplanted 250 nm thick samples using a SQUID magnetometer at 5 K. The magnetic field was applied along a direction parallel to the film plane.

3. Results and discussion

3.1. 250 nm thick films

Multi-step ion implantation was performed using N^+ and N_2^+ ions at various energies to obtain a suitable

TABLE I Conditions for each step of multi-step implantation and annealing for a 250 nm thick iron film

Step	Ion	Energy (keV)	Dose (10^{21} m^{-2})
1	N^+	150	2
2	N^+	100	2
3	N_2^+	100	1
4	N_2^+	50	1
5	Annealing at 423 K for 1 h		
6	N^+	175	2
7	N_2^+	100	1
	N_2^+	50	1

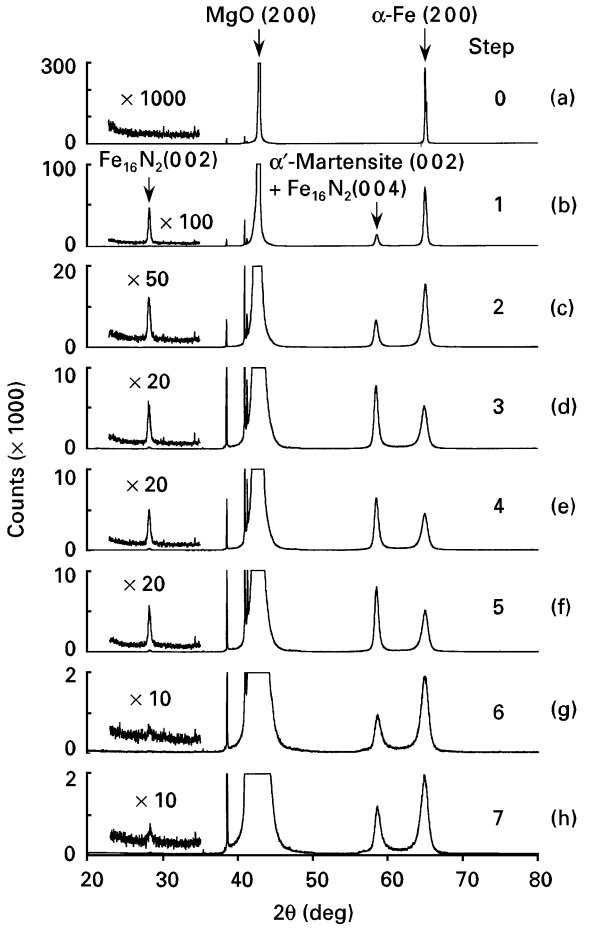

Figure 1 A series of X-ray diffraction spectra of 250 nm thick iron films after each step of multiple ion implantation and annealing.

nitrogen concentration throughout 250 nm thick films. The implantation or the annealing condition in each step is shown in Table I.

Fig. 1 shows a series of the XRD patterns obtained before and after each step of the multi-step implantation. Fig. 1a shows the XRD pattern of 250 nm thick iron films before implantation (step 0). In addition to the MgO(200) line, a sharp Fe(200) line was observed, showing a strong [100] preferred orientation of the film perpendicular to the film plane. Fig. 2 shows depth profile of nitrogen concentration for each step of the implantation, which was calculated by the LSS theory [16] assuming gaussian distribution. In this case, the effects of, for example, surface recession

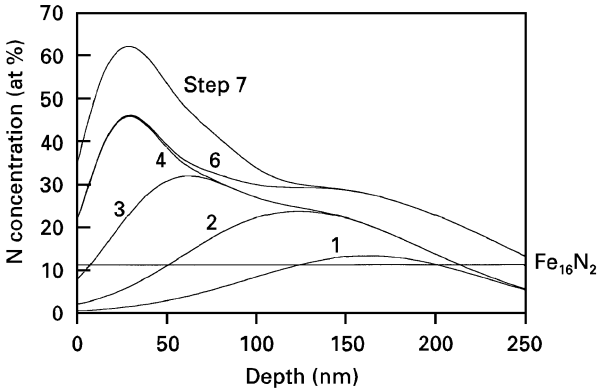

Figure 2 Calculated depth profile of nitrogen concentration after each step of multiple ion implantation of 250 nm thick iron films.

by sputtering, nitrogen escape from the surface and redistribution of nitrogen atoms during ion irradiation, were not taken into account. It can be seen in the figure that the depth region of nitrogen concentration is larger than that of α″-$Fe_{16}N_2$ (11.1%) extends significantly with increasing implantation step.

In step 1, the α-Fe(200) line decreased in intensity, while the α′-martensite(002) peak overlapped with α″-$Fe_{16}N_2$(004) peak and the α″-$Fe_{16}N_2$(002) peak appeared (Fig. 1b). The volume fractions of these phases were estimated from the integrated XRD intensities according to the method shown in the Appendix. From step 1 to step 3, the relative XRD intensity of the α′(002) + α″(004) line and the α″-$Fe_{16}N_2$(002) line increased with implantation step, while that of the α-Fe(200) line decreased (Fig. 1b–d). In step 4, the relative XRD intensity of α′-martensite or α″-$Fe_{16}N_2$ became a maximum and the maximum volume fraction of α′ + α″ or α″ was estimated to be 51% or 12%, respectively (Fig. 1e).

In step 5, the film was annealed at 423 K for 1 h, but the volume fraction of α′-martensite or α″-$Fe_{16}N_2$ was almost saturated. This may be due to the presence of residual α-Fe crystals near the deepest region of the film (Fig. 1f). Thus, in step 6, nitrogen ions were implanted at a higher energy of 175 keV in order to supply nitrogen atoms in the deepest region. However, the volume fractions of both the nitride phases were found to decrease (Fig. 1g). This may result from a fact that a considerable amount of nitrogen atoms in the shallow depth region diffused out from the surface under deep implantation conditions. In step 7, nitrogen ions were implanted at a low energy of 50 keV to compensate nitrogen atoms in the shallow depth region. As a result, the volume fractions of both the nitrides increased slightly (Fig. 1h).

From these experimental results, it can be concluded that multi-step implantation should be carried out with different ion energies in the order of decreasing energies or ion ranges (from deeper to shallower depth regions). If the order of the implantation is reversed, previously implanted nitrogen atoms near the surface will be released by radiation-enhanced diffusion.

Fig. 3 shows the calculated depth profile of nitrogen concentration after multi-step implantation (step 4),

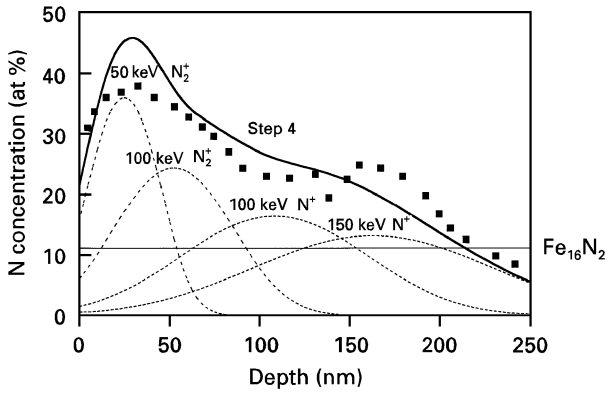

Figure 3 Depth profile of nitrogen concentration measured by Auger electron spectroscopy (■). (——) Depth profile for step 4.

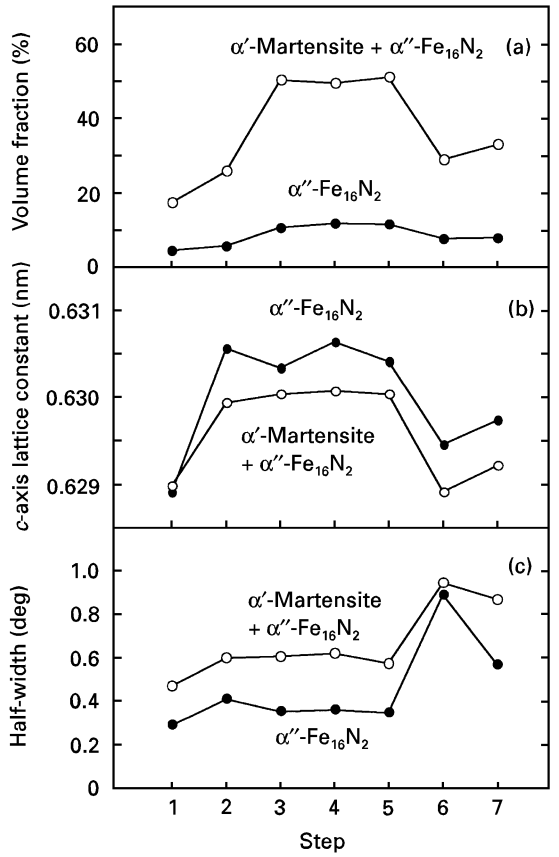

Figure 4 Change of (a) the volume fractions of $\alpha' + \alpha''$ and α'', (b) the *c*-axis lattice constants of $\alpha' + \alpha''$ and α'', and (c) the half-widths of α' (0 0 2) + α'' (0 0 4) and α'' (0 0 2) reflections with multiple ion implantation and annealing.

and the experimental data obtained by Auger electron spectroscopy combined with argon ion etching. Although the Auger data are only qualitative, both the curves coincide well with each other in a reasonable manner.

Fig. 4a shows variation of the volume fractions of $\alpha' + \alpha''$ and α'' with multi-step implantation. The volume fraction of $\alpha' + \alpha''$ increased from step 1 to step 3 and reached a maximum between steps 3 and 5. Then it decreased steeply from step 5 to step 6 and slightly increased from step 6 to step 7. Fig. 4b shows changes of the *c*-axis lattice constants of $\alpha' + \alpha''$ and α''. The increase of the lattice constants from step 1 to step 2 shows that nitrogen concentration in α'-martensite and α''-$Fe_{16}N_2$ phases increased with increasing number of steps. From step 2 to step 4, the lattice constant remained almost unchanged. The maximum value of the lattice constant of α''-$Fe_{16}N_2$ was a little larger than the previously reported value [17]. The deep implantation in step 6 caused the lattice constant to decrease significantly, suggesting the decrease of nitrogen concentration in α'-martensite and α''-$Fe_{16}N_2$ phases due to the loss of nitrogens from the surface region during the deep implantation. Fig. 4c shows change of the half-widths of α'(0 0 2) + α''(0 0 4) peak and α''-$Fe_{16}N_2$(0 0 2) peak. The half-widths were relatively small from step 1 to step 5, but increased abruptly in step 6. This suggests that high-energy ion implantation induces radiation damage in the nitride phases, or causes shrinkage of the nitride crystal to a small size with decreasing nitrogen concentration in the near surface region.

Fig. 5 shows magnetic hysteresis curves of 250 nm thick iron films unimplanted and implanted with nitrogen ions. For the implanted specimen, the volume fractions of α'-martensite and α''-$Fe_{16}N_2$ were 47% and 0.8%, respectively. The saturation magnetization observed was larger than that of unimplanted one by 5% and was 2.3 T. Assuming that the saturation magnetization of the sample is a weighted average of those of $\alpha' + \alpha''$ and α-Fe, the saturation magnetization of $\alpha' + \alpha''$ was estimated to be 2.4 T. Coercive force was increased to about 16 kA m^{-1} by the ion implantation.

3.2. 50 nm thick films

In order to examine the effects of film thickness on the formation of α''-$Fe_{16}N_2$, 50 nm thick iron films were implanted with nitrogen ions and compared with 250 nm thick films. Table II shows the implantation or the annealing condition in each step of the multi-step process.

Fig. 6 shows a series of XRD patterns of 50 nm thick iron films. Before ion implantation, only a strong α-Fe(2 0 0) peak was observed, indicating a strong [1 0 0] preferred orientation of the film (Fig. 6a). After implantation of 50 keV N_2^+ ions to a dose of 5×10^{20} m^{-2}, the α'-martensite(0 0 2) peak appeared and the α-Fe(2 0 0) peak decreased in intensity (Fig. 6b). The volume fraction of α'-martensite was estimated to be about 66%. After additional implantation of 25 keV N_2^+ ions to a dose of 5×10^{20} m^{-2}, the α-Fe(2 0 0) peak became very small (Fig. 6c). The volume fraction of α'-martensite exceeded 90%, but α''-$Fe_{16}N_2$(0 0 2) was not observed.

Fig. 7 shows the calculated depth profile of nitrogen concentration after the double-step ion implantation, together with the Auger depth profile. Both the depth profiles coincide well with each other.

The nitrogen-ion implanted 50 nm thick films were annealed in vacuum at temperatures between 423 and 573 K for durations between 10 s and 756 ks. In order to prevent nitrogen escaping from the surface,

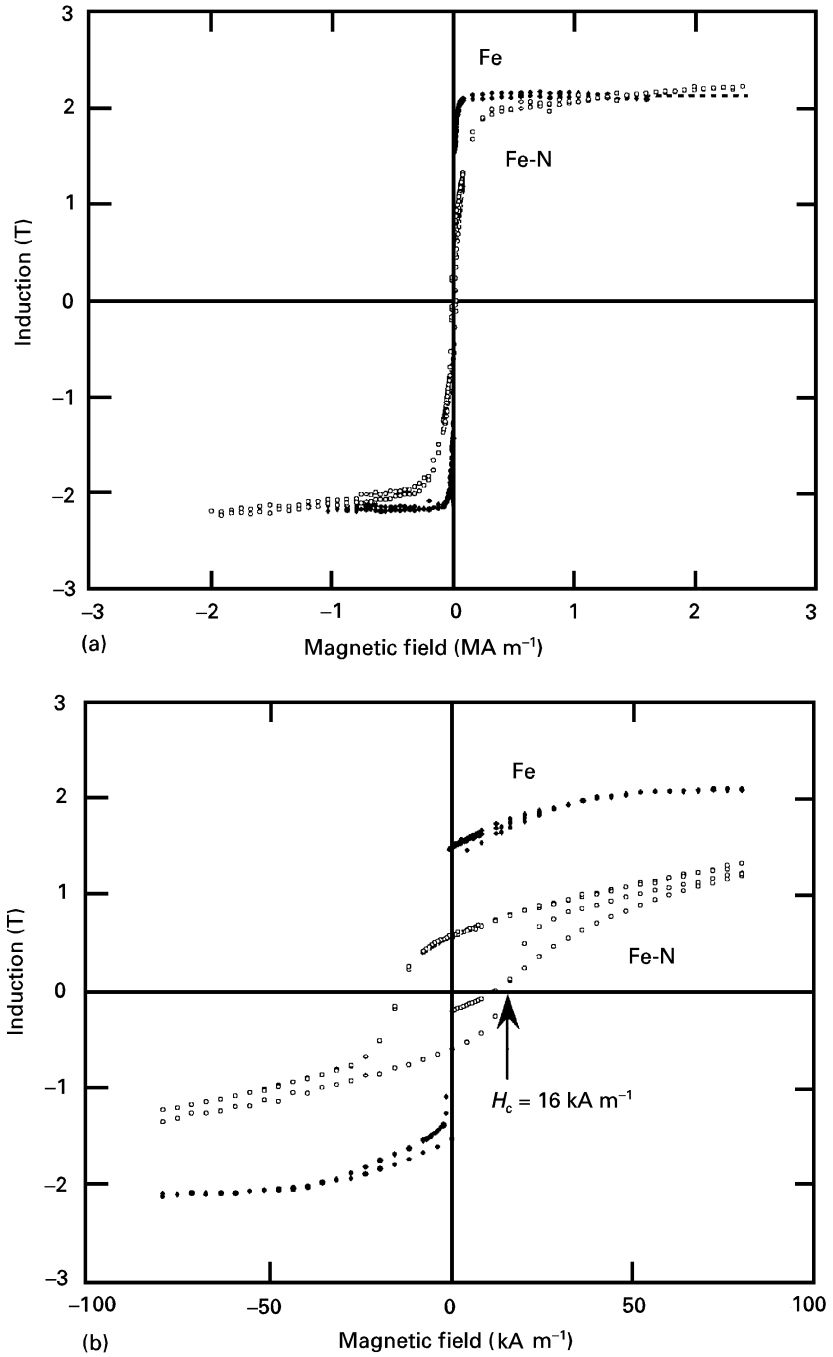

Figure 5 (a) Magnetic hysteresis curves of 250 nm thick iron films unimplanted and implanted with 150 keV N^+ ions to a dose of 2×10^{21} m^{-2}, 100 keV N^+ ions to 8×10^{20} m^{-2} and 100 keV N_2^+ ions to 1×10^{21} m^{-2}, respectively. (b) Enlargement of part of the figure.

TABLE II Conditions for each step of multi-step implantation and annealing for a 50 nm thick iron film

Step	Ion	Energy (keV)	Dose (10^{20} m^{-2})
1	N_2^+	50	5
2	N_2^+	25	5
3	Coating with copper or gold films		
4	Annealing at 423 K for 1 h		
5	Annealing at 423 K for 10 h		

implanted specimens were coated with gold or copper films, about 50 nm thick before annealing.

α''-$Fe_{16}N_2$(0 0 2) peak appeared in the XRD pattern of the specimen coated with copper film and annealed at 437 K for 10 h (Fig. 6f). The volume fraction of α''-$Fe_{16}N_2$ reached 36%. Fig. 8 shows an example of the XRD patterns of uncoated and gold-coated specimens after annealing at 437 K for 200 h. Although a Au(2 2 0) peak overlapped with that of α-Fe(2 0 0), α''-$Fe_{16}N_2$(0 0 2) peak was clearly observed in the gold-coated specimen but not in the uncoated specimen. The peak intensity of α'(0 0 2) + α''(0 0 4) for the gold-coated specimen was much larger than that of the uncoated specimen. In the coated specimen, nitrogen concentration was kept high enough to transform α'-martensite to α''-$Fe_{16}N_2$. In the uncoated specimen, a γ'-Fe_4N(2 2 0) peak was observed.

Thus, we obtained a relationship between the observed phase and the annealing condition, as shown in

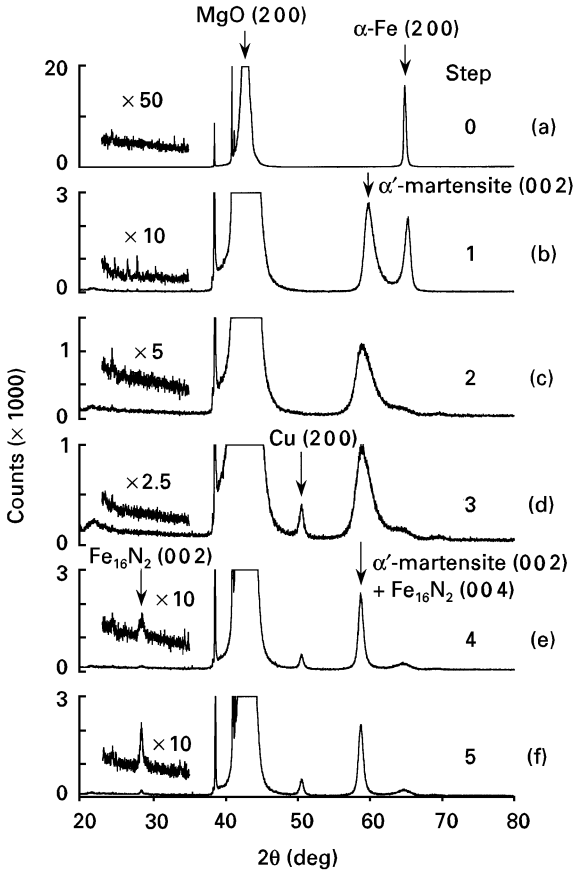

Figure 6 A series of X-ray diffraction spectra of 50 nm thick iron films after each step of multiple ion implantation and annealing.

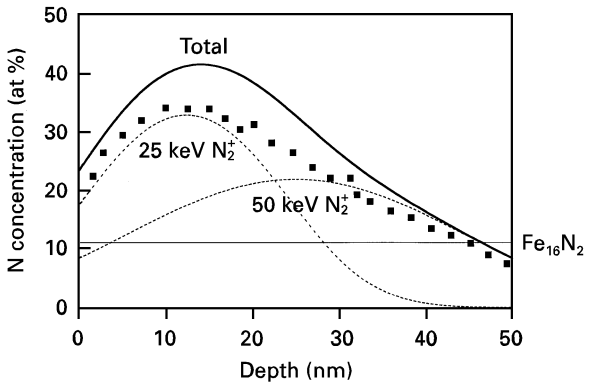

Figure 7 Calculated depth profile of nitrogen concentration for each step of multiple ion implantation and the Auger profile (■).

Fig. 9. The annealing temperature–time diagram was divided into three regions according to the phase change. In region A, no change in the XRD pattern was observed. The annealing time was too short to cause structural changes in specimens. In region B, the α″-$Fe_{16}N_2$(002) peak appeared and increased in intensity with increasing annealing time. Optimum annealing time became shorter with increasing annealing temperature. In region C, the α″-$Fe_{16}N_2$(002)

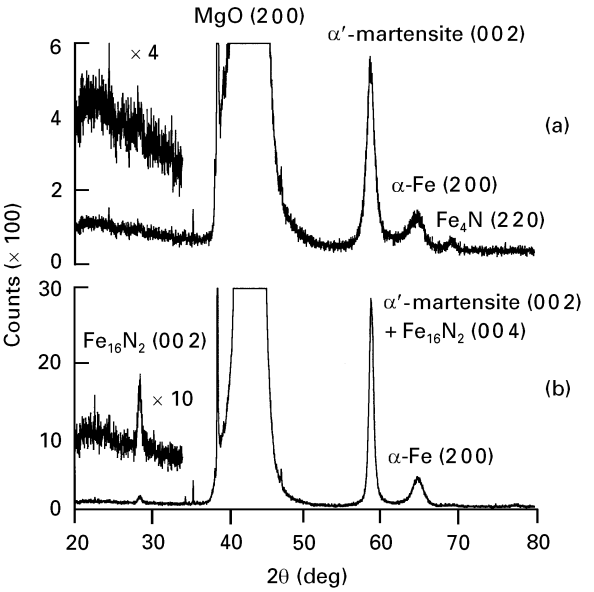

Figure 8 X-ray diffraction pattern of 50 nm thick specimens (a) uncoated and (b) coated with gold films after annealing at 437 K for 200 h.

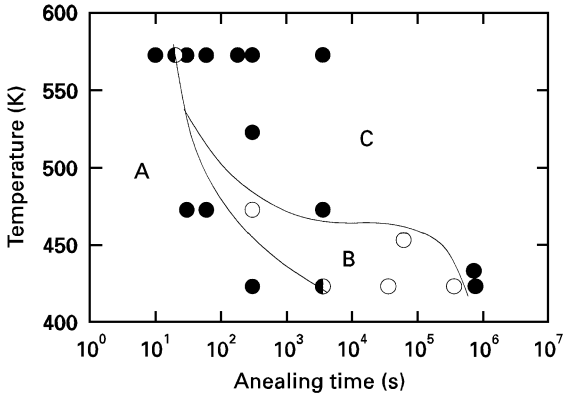

Figure 9 Annealing temperature–time diagram. (○) Formation or (●) no formation of α″-$Fe_{16}N_2$.

disappeared and the α′-martensite(002) peak became smaller, while the α-Fe(200) peak became larger. In some cases, small peaks due to ε-$Fe_{2-3}N$ and γ′-Fe_4N nitrides appeared.

Fig. 10b shows change of the *c*-axis lattice constants of α′, α′ + α″ and α″ phases with increasing number of steps. The lattice constant of α′ just after ion implantation was obviously smaller than that in 250 nm thick films. This indicates the nitrogen concentration of the α′-martensite is smaller than that in 250 nm thick films. In step 4, an α″-$Fe_{16}N_2$(002) peak appeared when the lattice constant increased with annealing.

In Fig. 10c, the half-width of the α′-martensite(002) line in the as-implanted state was very large and the line shape was asymmetric. This suggests that the α′-martensite phase contains a wide range of nitrogen concentrations. The half-width of the α′-martensite(002) line decreased after annealing. This may be due to the formation of α″-$Fe_{16}N_2$ phase.

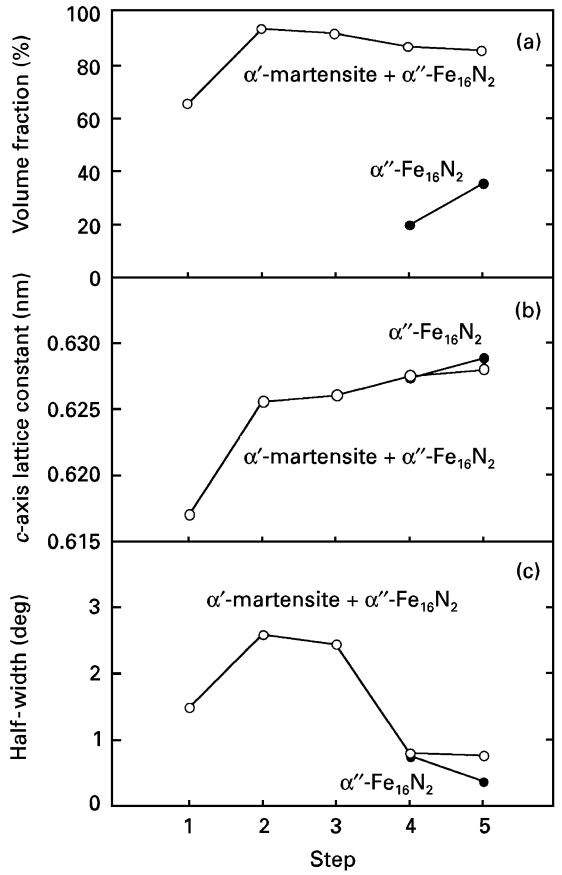

Figure 10 Change of (a) the volume fractions of $\alpha' + \alpha''$ and α'', (b) the *c*-axis lattice constants of $\alpha' + \alpha''$ and α'', and (c) the half-widths of α' (0 0 2) + α'' (0 0 4) and α'' (0 0 2) reflections with multiple ion implantation and annealing.

4. Conclusion

In order to create a metastable α''-$Fe_{16}N_2$ phase, (1 0 0)-oriented iron thin films were implanted with nitrogen ions at room temperature. For 250 nm thick specimens, α''-$Fe_{16}N_2$ was formed by nitrogen-ion implantation. Sequential multiple ion implantation increased the volume fraction of α''-$Fe_{16}N_2$ when nitrogen ions were implanted from deep to shallow regions by decreasing the ion energies or ion ranges. The maximum volume fractions of α''-$Fe_{16}N_2$ and α'-martensite + α''-$Fe_{16}N_2$ were 12% and 51%, respectively. Magnetic measurement showed that the saturation magnetization of a mixed phase of $\alpha' + \alpha''$ was 2.4 T.

For 50 nm thick specimens, no α''-$Fe_{16}N_2$ but α'-martensite was formed after the ion implantation, and the volume fraction of α'-martensite exceeded 90%. α''-$Fe_{16}N_2$ was formed by postannealing, when the implanted specimens were coated with copper or gold films. The maximum volume fraction of α''-$Fe_{16}N_2$ reached 36%.

Acknowledgement

The authors thank Dr K. Yabe, Hokkaido National Industrial Research Institute, for Auger depth profile measurements.

Appendix

The volume fractions of α-Fe, α′-martensite and α″-$Fe_{16}N_2$ were estimated from the measured integrated intensities of X-ray diffraction peaks as

$$V_\alpha = I_{\alpha(200)}/(I_{\alpha(200)} + I_{\alpha'(002)+\alpha''(004)})$$

$$V_{\alpha'+\alpha''} = I_{\alpha'(002)+\alpha''(004)}/(I_{\alpha(200)} + I_{\alpha'(002)+\alpha''(004)})$$

$$V_{\alpha''} = I_{\alpha''(002)}/k/(I_{\alpha(200)} + I_{\alpha'(002)+\alpha''(004)})$$

where V_α, $V_{\alpha'+\alpha''}$ and $V_{\alpha''}$ are the volume fractions of α-Fe, α′-martensite + α″-$Fe_{16}N_2$, and α″-$Fe_{16}N_2$, respectively. $I_{\alpha(200)}$, $I_{\alpha'(002)+\alpha''(004)}$, and $I_{\alpha''(002)}$ are the integrated intensities of α-Fe(2 0 0), α′-martensite(0 0 2) overlapped with α″-$Fe_{16}N_2$(0 0 4), and α″-$Fe_{16}N_2$(0 0 2), respectively.

The constant, k, is the theoretical ratio of the intensity of α″-$Fe_{16}N_2$(0 0 2) peak to that of α″-$Fe_{16}N_2$(0 0 4) peak and is calculated as follows.

The integrated intensity of the ($h\,k\,l$) reflection, I_{hkl}, is given by

$$I_{hkl} = |F_{hkl}|^2 p L_p, \qquad \text{(A1)}$$

where F_{hkl}, p, and L_p represent structure factor, multiplicity factor, and Lorents polarization factor, respectively [18]. In the case of a single crystal, the multiplicity factor becomes 1. The Lorents polarization factor, L_p, will be

$$L_p = (1 + \cos^2 2\theta)/(\sin\theta \cos\theta) \qquad \text{(A2)}$$

instead of the following equation for polycrystal

$$L_p = (1 + \cos^2 2\theta)/(\sin 2\theta \cos\theta) \qquad \text{(A3)}$$

where θ is the Bragg angle. For highly (0 0 1) oriented samples, as in the present case, the k value is calculated to be 0.074 instead of 0.148 for randomly oriented polycrystal.

References

1. T. K. KIM and M. TAKAHASHI, *Appl. Phys. Lett.* **20** (1972) 492.
2. H. SHOJI, H. TAKAHASHI, M. KUNII, M. TAKAHASHI and T. WAKIYAMA, *J. Magn. Soc. Jpn* **17** (1993) 323.
3. M. TAKAHASHI, H. SHOJI and M. TSUNODA, *J. Magn. Magn. Mater.* **134** (1994) 403.
4. M. KOMURO, Y. KOZONO, M. HANAZONO and Y. SUGITA, *J. Appl. Phys.* **67** (1990) 5126.
5. Y. SUGITA, K. MITSUOKA, M. KOMURO, H. HOSHIYA, Y. KOZONO and M. HANAZONO, *ibid.* **70** (1991) 5977.
6. M. Q. HUANG, W. E. WALLACE, S. SIMIZU, A. T. PEDZIWIATR, R. T. OBERMYER and S. G. SANKAR, *ibid.* **75** (1994) 6574.
7. A. MORISAKO, K. TAKAHASHI, M. MATSUMOTO and M. NAOE, *ibid.* **63** (1988) 3230.
8. C. GAO, W. DOYLE and M. SHAMSUZZOHA, *ibid.* **73** (1993) 6579.
9. K. NAKAJIMA, S. OKAMOTO and T. OKADA, *ibid.* **65** (1989) 4357.
10. K. NAKAJIMA and S. OKAMOTO, *Appl. Phys. Lett.* **54** (1989) 2536.
11. *Idem*, *ibid.* **56** (1990) 92.

12. K. NAKAJIMA, T. YAMASHITA, M. TANAKA and S. OKAMOTO, *J. Appl. Phys.* **70** (1991) 6033.
13. H. SHINNO, K. SAITO and M. UEHARA, in "Proceedings of the 10th Symposium on Surface Layer Modification by Ion Implantation", edited by M. Iwaki (IONICS publish. Co. Ltd., Tokyo, 1994) pp. 17–23.
14. K. MITSUOKA, H. MIYAJIMA, H. INO and S. CHIKAZUMI, *J. Phys. Soc. Jpn* **53** (1984) 2381.
15. A. SAKUMA, *J. Magn. Magn. Mater.* **102** (1991) 127.
16. J. LINDHARD, M. SCHARFF and H. E. SCHIØTT, *Fys. Medd. K. Dan. Vidensk.* **33** (1963) 1.
17. K. H. JACK, *Proc. R. Soc.* **A208** (1951) 216.
18. B. D. CULLITY, "Elements of X-ray Diffraction" (Addison-Wesley, Reading, 1978).

Received 5 June
and accepted 17 September 1996